Theoretical and Experimental Study of Piston Gas-Heating with Laminar Energy Losses

STELLAN KNÖÖS*
Northrop Corporate Laboratories, Hawthorne, Calif.

The effects of laminar heat-transfer losses on piston gas-heater performance have been studied theoretically and experimentally. For the analysis, the gas is separated into an isentropic "core" and a developing thermal layer over the "wetted" wall. The heat-transfer rate and thermal boundary-layer thickness are computed in a boundary-layer integral approach, using a zero-order similarity profile for the gas density. The equations were solved with the help of a digital computer and several interesting solutions were obtained. Experiments were conducted with helium and argon in a specially built gas compressor, with a pneumatically driven piston, generally performing one complete forward stroke and one reverse stroke. The experimentally measured time history of the gas pressure (i.e., the average energy density) was found to agree remarkably well with theoretical predictions. The presented computational scheme could potentially be applied to such shock tube and shock tunnel piston compressors where the piston velocity is much smaller than the speed of sound of the gas, as well as to a wide class of laminar gas flow devices using reciprocating pistons.

Nomenclature

A = wetted surface area
c_p = specific heat
d_0 = reference length, $d_0 = 4V_0/A_0$
D = piston diameter
E = total internal energy of gas
f = gas-density similarity function, $f(\eta) = (\rho - \rho_\infty)/(\rho_w - \rho_\infty)$
g = dimensionless piston-motion function, $\tilde{t} = g(\xi)$
G = dimensionless function, defined in Eq. (14)
h = specific enthalpy
$\tilde{L}$ = dimensionless energy loss, defined in Eq. (24)
p = gas pressure
q = heat flux
$\tilde{q}$ = dimensionless heat flux, defined in Eq. (25)
Q_{loss} = total heat-transfer loss, defined in Eq. (19)
t = time from start of piston motion
T = temperature
$\tilde{u}$ = dimensionless piston velocity, defined in Eq. (25)
v = flow velocity perpendicular to the plane $y = 0$
V = compressor volume (time dependent)
$\tilde{W}$ = work addition parameter, defined in Eq. (23)
x = coordinate in the direction of piston motion
y = coordinate in the direction perpendicular to the wall
γ = specific-heat ratio
δ = boundary-layer thickness parameter
ϵ = main boundary-layer-growth parameter, defined in Eq. (25)
ϵ_{10} = modified boundary-layer-growth parameter, $\epsilon_{10} = \epsilon(1 - \tilde{t}_{10})^{1/2}$
η = dimensionless wall distance parameter, $\eta = y/\delta$
λ = thermal conductivity
ξ = dimensionless piston position, $\xi = x/x_0$
ρ = gas density
ψ = fraction of compressor volume occupied by boundary layer gas, defined in Eq. (27)

Subscripts

0 = reference condition at $\xi = 1.0$ for isentropic compression
1 = initial condition at time $t = 0$
w = condition at the wall
∞ = condition in the isentropic "core"
"1," "2," . . . "13" = marked piston position in experiment, defined in Fig. 3

Received May 28, 1970; revision received October 13, 1970. The author gratefully acknowledges the assistance of R. Tanquary in the experiments and G. Duckworth in the numerical analysis.

* Member Senior Technical Staff; presently consultant to Aeronautical Research Institute of Sweden (FFA), Bromma, Sweden. Member AIAA.

I. Introduction

HEATING of gases is commonly performed with the help of piston compressors. Pressure work from the moving piston is transferred to the gas, and the temperature of the gas raised according to the isentropic law $T \sim \rho^{\gamma-1}$, if the process is reversible. In real gas compressors, heat transfer to the walls will be present, and as a result the compression becomes irreversible with a lowering of the temperature and pressure, compared to isentropic values for the same over-all volumetric compression. For compressor applications, this is in fact the desired feature, and in order to minimize the work input, the heat transfer should be maximized (constant temperature compression). To accurately predict the spatial variation and variation in time of the gas properties within the compressor during the compression is a formidable task. At the present, no method or computational scheme with demonstrated ability to accurately predict an actual compression with heat losses is available in the literature.

Limiting the discussion to thermal boundary layers of laminar nature without gravitational convection as for rapid-heating devices, the over-all effect of heat transfer has been observed, e.g., in free-piston compressors (e.g., Williard[1] and Knöös[2,3]). Here losses have been found to be of extreme importance to the over-all performance of the compressor; they do in fact limit the practical usefulness of the free-piston heater generally to less than 8000°K for a gas with low-molecular weight if the problem is not given special attention and proper design features are incorporated. A most important and most hazardous property of the free-piston compressor suffering from high-energy losses is a very much higher peak pressure than an isentropic compression (no losses) with the same energy input to the free piston. It is of great importance for the further development of piston heaters and other piston compressors that schemes for computing the over-all effect of heat transfer be established, and their practical usefulness checked in experiments.

The present experimental and theoretical study focuses on piston compressions with unsteady laminar heat transfer to

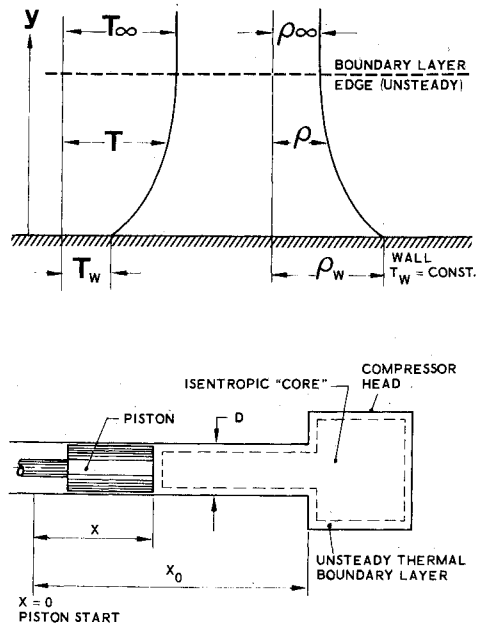

Fig. 1 Nomenclature for the unsteady thermal boundary layer (upper figure). Piston compressor geometry (lower figure).

a constant-temperature wall. The freestream (core) gas conditions are assumed to be spatially homogeneous, with the core gas temperature equal to the wall temperature at the start of a compression, and with given piston kinematics. Most attention will be given moderate volumetric compression ratios of the order ten, and real-gas effects not accounted for. The presented theory will utilize a simple similarity concept for the unsteady boundary layer for calculations of the heat flux. This flux is thereafter used in a "wetted-surface" model for the calculation of energy losses in the compressor. The presented computations are compared with measured pressure data from an experimental rig, specially designed for measurement of the heat-transfer effects, and several interesting features of the piston compressions quantitatively revealed.

II. Theory

Basic Assumptions

For simplicity, we consider a gas compressor with uniform thermodynamic conditions in the core outside a thermal boundary layer, as indicated in Fig. 1. The piston velocity is assumed small, and the gas velocities everywhere much smaller than the speed of sound. The momentum equation gives the trivial solution of uniform pressure in the compressor. The boundary-layer characteristics, including the unsteady heat flux to the walls, are assumed to be uniform over the wall. The gas properties are perfect with a constant value for the ratio of specific heats. At time $t = 0$ the piston motion is started with the gas temperature initially equal to the wall temperature. The product $(\lambda\rho c_p)$ for the wall material is considered to be very much larger than the corresponding quantity for the gas. Therefore, in the subsequent compression heating the wall temperature will not deviate substantially from the initial value.

The heat flux and the development of the thermal boundary layer in time will be computed from an integral energy equation, using a fictitious boundary layer developing over a flat infinite plate, much similar to the classical Rayleigh problem (Rayleigh,[4] Van Dyke[5]) or extensions thereof to thermal boundary layers of high-temperature real gases (e.g., Knöös[6]). The actual effect of compression or expansion of the boundary layer in a direction parallel to the wall is not accounted for in the present heat-flux calculation; in the analysis the heat flux will be computed for a case with gas motion solely in the direction perpendicular to the wall. This heat-transfer rate, as well as the boundary-layer thickness (which is a less important parameter here), used in an over-all energy integral for the compressor gas together with isentropic expressions for the gas in the "core," give a sufficient set of equations and possibility of computing the gas pressure and other parameters by stepwise in time forward-marching procedure. The analysis will be carried only through one forward and one reverse piston stroke.

Breakdown of the present analysis will occur when the boundary-layer thickness becomes so large that boundary layers from opposite walls in the compressor interact, or corner effects become important. In the computations we will therefore carefully keep a record of the computed boundary-layer thicknesses, noting that the boundary-layer thickness can reach temporary large maxima that violate our small thickness assumption, in spite of the thickness subsequently being acceptably small, e.g., near piston turning.

Boundary-Layer Equations

The conservation equations for mass and energy in the unsteady laminar boundary layer flow with small flow velocities can be written

$$\partial\rho/\partial t + (\partial/\partial y)(\rho v) = 0 \tag{1}$$

$$(\partial/\partial t)(\rho h) + (\partial/\partial y)(\rho v h) = (\partial/\partial y)(\lambda\partial T/\partial y) + dp/dt \tag{2}$$

Here, the gas density is denoted ρ, the pressure p (spatially uniform), the temperature T, the enthalpy h, and the thermal conductivity λ. The coordinate perpendicular to the wall is denoted y, and the gas velocity v, is positive in the y direction.

Integrating the energy equation across the boundary layer to an arbitrary coordinate y outside the boundary layer, we find

$$\frac{d}{dt}\int_0^y \rho h\, dy + (\rho v h)_\infty = q_w + y\frac{dp}{dt} \tag{3}$$

Here, subscript ∞ refers to the condition in the core, and q_w to the heat-transfer rate at the wall, $q_w = -(\lambda\partial T/\partial y)_w$. With the help of the equation for conservation of mass, Eq. (3) can be rewritten

$$q_w = \frac{d}{dt}\int_0^y \rho h dy - h_\infty\frac{d}{dt}\int_0^y \rho dy - y\frac{dp}{dt} \tag{4}$$

For a perfect gas we have

$$\rho h = [\gamma/(\gamma - 1)]p \tag{5}$$

and hence Eq. (4) becomes

$$-q_w = h_\infty\frac{d}{dt}\int_0^\infty \rho dy - \frac{1}{\gamma - 1}\, y\frac{dp}{dt} \tag{6}$$

With the thermodynamic conditions of the core changing according to the isentropic law, as assumed, we have $dp/dt = (\gamma p/\rho_\infty)d\rho_\infty/dt$. The wall heat-transfer rate can then be written in the following, simpler form

$$-q_w(t) = h_\infty(t)\frac{d}{dt}\int_0^\infty [\rho(t) - \rho_\infty(t)]dy \tag{7}$$

We introduce a zero-order similarity profile $f(\eta)$ for the density distribution within the boundary layer

$$[\rho(t) - \rho_\infty(t)]/[\rho_w(t) - \rho_\infty(t)] = f(\eta); \quad \eta = y/\delta(t) \tag{8}$$

where $\delta(t)$ is a characteristic boundary-layer thickness. The similarity function $f(\eta)$ satisfies the conditions $f(0) =$

1 and $f(\infty) = 0$. An alternate form for the wall heat-transfer rate is then

$$q_w = \lambda_w f'(\eta = 0)(T_w/\delta)(1 - \rho_\infty/\rho_w) \tag{9}$$

where subscript w denotes the condition at the wall. Inserting this result into Eq. (7), the following differential equation for the boundary-layer thickness is found

$$\frac{d}{dt}\left[\delta\rho_w\left(1 - \frac{\rho_\infty}{\rho_w}\right)\right]^2 = \frac{-2\lambda_w f'(\eta = 0)}{\int_0^\infty f(\eta)dy}\frac{T_w\rho_w}{h_\infty}\left(1 - \frac{\rho_\infty}{\rho_w}\right)^2 \tag{10}$$

We choose initial values at $t = 0$ to be

$$t = 0: \qquad p = p_1; \quad T_w = T_1; \quad T_\infty = T_1 \tag{11}$$

With isentropic freestream conditions and constant temperature of the wall we also have

$$\frac{p(t)}{p_1} = \left[\frac{T_\infty(t)}{T_w}\right]^{\gamma/(\gamma-1)} = \left[\frac{\rho_w(t)}{\rho_\infty(t)}\right]^{\gamma/(\gamma-1)} \tag{12}$$

The differential equation can be integrated to yield the following expression for the boundary-layer thickness

$$\delta(t) = \left\{\frac{-2f'(\eta = 0)}{\int_0^\infty f(\eta)d\eta}\left(\frac{\lambda}{\rho c_p}\right)_1\left(\frac{T_w}{T_\infty}\right)^{2\gamma/\gamma-1} \times \frac{tG(t)}{[1 - (T_w/T_\infty)]^2}\right\}^{1/2} \tag{13}$$

Here $G(t)$ is a dimensionless function (generally having weak variation with time(t)

$$G(t) \equiv \frac{1}{t}\int_0^t \frac{(1 - T_w/T_\infty)^2}{(T_w/T_\infty)^{1/(\gamma-1)}}\,dt \tag{14}$$

Corresponding expression for the heat-transfer rate at the wall is

$$q_w(t) = \mp\left(\frac{-f'(\eta = 0)\int_0^\infty f(\eta)d\eta)}{2}\right)^{1/2} \times T_1(\lambda\rho c_p)_1^{1/2}\frac{(1 - T_w/T_\infty)^2}{(T_w/T_\infty)^{\gamma/(\gamma-1)}}\frac{1}{[tG(t)]^{1/2}} \tag{15}$$

The negative sign should be used when $T_w/T_\infty < 1$, and the positive sign when $T_w/T_\infty > 1$.

The similarity function $f(\eta)$ has not been specified. From the conservation equations it is possible to derive the following relation, which should hold true at the wall of the compressor

$$(\partial/\partial y)(\lambda\partial T/\partial y)_w = -dp/dt \tag{16}$$

For our purpose, this could be rewritten in the more appropriate form

$$(\partial/\partial\eta)[(\lambda/\lambda_w)(\partial/\partial\eta)(\rho_w/\rho)]_w = -(\delta^2/\lambda_w T_w)dp/dt \tag{17}$$

We see that the real density profile is affected by the temperature dependence of the thermal conductivity, and by the value for the dimensionless parameter $[(\delta^2/\lambda_w T_w)dp/dt]$. It is possible to account for nonsimilarity in the boundary layer profile by using, e.g., a one-parameter density profile and a von Kármán-Pohlhausen technique (see Schlichting[7]). However, the heat-transfer calculation is not very sensitive to a change in the boundary layer profile, and for the present purposes the zero-parameter calculation will be considered adequate.

In the analysis we assume

$$f'(\eta = 0)\int_0^\infty f(\eta)d\eta = -1.0$$

and $f'(\eta = 0) = -1.0$. The first parameter is most important for the heat flux calculation, and the second parameter of minor importance and needed for an estimate of the boundary layer thickness. It is interesting to note that

$$f'(\eta = 0)\int_0^\infty f(\eta)d\eta$$

takes the value -1.0 for such different density profiles as the exponential $f(\eta) = \exp(-\eta)$, and $f(\eta) = \cos(\pi/2)\eta$ with $\eta \leq 1.0$.

Over-All Energy Equation

The energy conservation equation for gas trapped in the piston compressor can be written

$$E - E_1 = \frac{\pi D^2}{4}\int_0^x p dx - Q_{\text{loss}} \tag{18}$$

where

$$Q_{\text{loss}} = -\int_0^t q_w(t)A(t)dt \tag{19}$$

Here, E is the total internal energy of the gas, x the piston position coordinate, as shown in Fig. 1, D the diameter of the circular piston, Q_{loss} the total energy loss from heat transfer, computed from the initiation of the forward piston stroke at $t = 0$, and $A(t)$ the exposed inner area of the compressor (the "wetted" area). Denoting x_0 the total length of the forward piston stroke, V_1 the initial compressor volume, V_0 the compressor volume at the end of the forward piston stroke, and A_0 corresponding "wetted" area, the following geometrical relation is valid

$$A(x) = A_0 + (4/D)(V_1 - V_0)(1 - x/x_0) \tag{20}$$

Using a characteristic length d_0, defined as $d_0 = 4V_0/A_0$, and introducing $\xi \equiv x/x_0$, the nondimensional "wetted" area becomes

$$A(\xi) \equiv A(\xi)/A_0 = 1 + (d_0/D)(V_1/V_0 - 1)(1 - \xi) \tag{21}$$

Eq. (18) can then be written in the dimensionless form

$$E/E_1 = 1 + [(V_1/V_0)^{\gamma-1} - 1][\tilde{W}(\xi) - \tilde{L}(\xi)] \tag{22}$$

Here, the work addition parameter $\tilde{W}(\xi)$ is defined as

$$\tilde{W}(\xi) \equiv \frac{\frac{\pi D^2}{4}\int_0^x p dx}{E_0 - E_1} = (\gamma - 1)\left(\frac{V_1}{V_0}\right)^\gamma \times \frac{1 - \frac{V_0}{V_1}}{(V_1/V_0)^{\gamma-1} - 1}\int_0^\xi \tilde{p}d\xi \tag{23}$$

and the heat loss parameter $\tilde{L}(\xi)$ defined as

$$\tilde{L}(\xi) \equiv \frac{Q_{\text{loss}}}{E_0 - E_1} = \epsilon\frac{\gamma 2(2)^{1/2}}{(V_1/V_0)^\gamma[1 - (V_0/V_1)^{\gamma-1}]}\int_0^\xi \tilde{q}\tilde{A}\,\frac{d\xi}{\tilde{u}} \tag{24}$$

The parameter E_0 is a reference energy, equal to the energy content of the gas for piston position $\xi = 1$ in a fictitious compression without energy losses. Remaining parameters are defined as

$$\tilde{u} = (\tau/x_0)dx/dt; \; \epsilon = (1/d_0)(\lambda/\rho c_p)_1^{1/2}\tau^{1/2}$$
$$\tilde{q} = \frac{q}{q_{\text{ref}}}; \quad q_{\text{ref}} = -\frac{T_1(\lambda\rho c_p)_1^{1/2}}{(2)^{1/2}\tau^{1/2}}; \quad \tilde{p} = \frac{p}{p_0} \tag{25}$$

The characteristic time τ is the duration of the forward piston stroke, the dimensionless piston velocity is $\tilde{u}$, and the reference heat-transfer rate is q_{ref}. The dimensionless param-

Table 1 Typical results from a numerical integration with $\epsilon = 0.20$, $\gamma = \frac{5}{3}$, $V_1/V_0 = 8.5$ and $d_0/D = 0.57$

ξ	$\tilde{t}$	ρ_∞/ρ_1	p/p_1	T_∞/T_1	E/E_1	$\tilde{W}$	$\tilde{L}$	$100G$	ψ	$\tilde{q}$	$\tilde{A}$
0	0	1	1	1	1	0	0	0	0	0	5.28
0.2	0.619	1.18	1.31	1.11	1.08	0.043	0.018	0.003	0.250	0.316	4.42
0.4	0.727	1.47	1.90	1.29	1.23	0.101	0.029	0.008	0.137	1.27	3.57
0.6	0.824	1.96	3.07	1.57	1.45	0.190	0.049	0.023	0.101	2.89	2.71
0.8	0.906	3.03	6.35	2.09	1.87	0.353	0.079	0.064	0.065	7.21	1.86
0.9	0.948	4.24	11.1	2.62	2.28	0.508	0.103	0.111	0.047	13.1	1.43
1.0	1	7.18	26.7	3.72	3.14	0.825	0.148	0.241	0.029	29.1	1.00
0.9	1.052	4.02	10.2	2.53	2.09	0.523	0.179	0.360	0.084	6.02	1.43
0.8	1.094	2.79	5.53	1.98	1.63	0.385	0.187	0.387	0.186	2.08	1.86
0.6	1.176	1.73	2.49	1.44	1.17	0.248	0.193	0.387	0.637	0.347	2.71
0.4	1.273	...	1.46	...	0.945	0.177	0.194	0.363	2.25	0.042	3.57
0.2	1.381	...	0.98	...	0.804	0.133	0.194	0.335	208	0.000	4.42
0	2	...	0.71	...	0.710	0.102	0.193	0.234	4.61	−0.022	5.28

eter ϵ is a measure of a thermal boundary-layer thickness-growth in the gas of reference pressure and temperature in a time interval τ, divided by the characteristic length d_0 of the compressor geometry. In summary, the parameters of the problem are $\epsilon, V_1/V_0$, d_0/D and γ.

The energy per unit volume of the gas is equal to $p/(\gamma - 1)$, and hence not varying spatially. The following important relation is therefore valid

$$p(t)/p_1 = (E/E_1)1/[1 - (1 - V_0/V_1)\xi] \qquad (26)$$

In the numerical analysis, the gas pressure is computed from Eq. (26), with the energy ratio E/E_1 given by Eq. (22).

Numerical Results

The described equations were used for computing the thermal boundary-layer development in the piston compressors, using a variety of combinations of independent parameters. The piston motion was given independently. It was specified by a normalized function $\tilde{t} = g(\xi)$, where $\tilde{t} = t/\tau$, and generally taken as measured in the experiments described in the following section. In the numerical analysis the equations were solved with a step-by-step finite difference technique with "open" formulas for computing the integrals. The forward stroke was generally divided in 100 steps or more, with smaller step size near the piston turning point. The reverse stroke was generally not taken

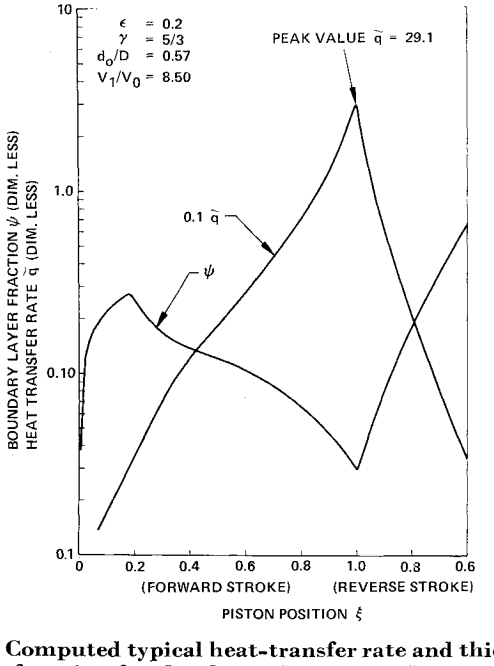

Fig. 2 Computed typical heat-transfer rate and thickness function for the thermal boundary layer.

symmetric in time with respect to the forward stroke; in the experiments the reverse strokes were slower. The numerical accuracy was carefully checked against exact solutions in "dry runs" with no heat transfer, and the accuracy was usually better than typically 10^{-3} in the peak pressure ratio, which is a most sensitive parameter (and also experimentally measured). The computational scheme was rapid. In fact, to perform one calculation of one forward and one reverse stroke typically required only one second on a CDC 6600 digital computer.

In the numerical analysis, the boundary layer thickness was expressed by the nondimensional parameter $\psi(t)$, defined as

$$\psi \equiv \frac{\delta(t)A(\xi)}{V(\xi)} = \frac{4\tilde{A}\delta/d_0}{\frac{V_1}{V_0} - \left(\frac{V_1}{V_0} - 1\right)\xi} \qquad (27)$$

With the density profile in the boundary layer equal to $f(\eta) = \exp(-\eta)$, the boundary layer will occupy all the compressor volume when $\psi \simeq 0.5$. Hence, in order for the present theory to be valid, the thickness parameter ψ should definitely satisfy the relation $\psi < 0.5$. In the performed analysis this condition was generally true in the forward stroke for low and moderate values of the main parameter ϵ. In the reverse stroke, the condition was violated, at least when the computed freestream temperature approached the value $T_\infty/T_1 = 1.0$. Here the breakdown of the small-thickness assumption is judged not to be of serious nature for a continued indicative calculation of pressure and energy according to Eqs. (22) and (26), back to the initial piston position $\xi = 0$, since the energy loss-rate near breakdown was generally small, and the loss parameter $\tilde{L}(\xi)$ nearly constant.

Results from a numerical integration are summarized in Table 1 for $\epsilon = 0.20$, $\gamma = \frac{5}{3}$, $V_1/V_0 = 8.5$, and $d_0/D = 0.57$. The function $g(\xi)$ was chosen similar to an experimentally measured profile. For simplicity it was taken to be symmetric around $\tilde{t} = 1$, and as in all the simulated experimental tests, the forward and reverse strokes were each divided into a sequence of five linear motions. The computed peak pressure at the piston turning point is $p(\xi = 1)/p_1 = 26.7$, considerably lower than the isentropic value $p/p_1 = 35.4$ for no losses. For $\xi = 1.0$ we find the energy ratio E/E_1 to be approximately 15% lower than the value for the temperature ratio T_∞/T_1, and that the thermal boundary layer occupies approximately 6% of the volume.

The peak volumetric compression-ratio for the freestream gas is $\rho_\infty/\rho_1 = 7.18$, and hence lowered from the given overall ratio $V_1/V_0 = 8.50$ by accumulation of cold and denser gas in the boundary layer. At $\xi = 1.0$ the work addition parameter takes the value $\tilde{W} = 0.825$, which is substantially lower than the loss-free value $\tilde{W} = 1.0$. In the reverse stroke the gas returns a smaller amount of pressure work to the piston than it received from the piston in the forward

Table 2 Numerical results, varying ϵ, d_0/D, and V_1/V_0 with $g(\xi)$ as in Table 1

			$\xi = 1.0$ Piston turning-point parameters							ξ	p/p_1
ϵ	d_0/D	V_1/V_0	ρ_∞/ρ_1	p/p_1	T_∞/T_1	E/E_1	$\tilde{W}$	$\tilde{L}$	ψ	$(\tilde{q} = 0)$	$(\xi = 0)$
0			8.50	35.4	4.16	4.16	1	0	0	0	1
0.05			8.13	32.9	4.04	3.87	0.948	0.043	0.006	0.06	0.91
0.10			7.79	30.6	3.93	3.60	0.903	0.081	0.013	0.11	0.84
0.20	0.57	8.50	7.18	26.7	3.72	3.14	0.825	0.148	0.029	0.21	0.71
0.40			6.16	20.7	3.36	2.44	0.703	0.249	0.070	0.36	0.55
0.60			5.36	16.4	3.06	1.93	0.613	0.319	0.124	0.48	0.49
0.80			4.71	13.3	2.81	1.56	0.545	0.368	0.192	0.57	0.48
0.40	0.10		6.97	25.4	3.65	3.04	0.824	0.180	0.060	0.24	0.67
0.40	0.50	8.50	6.28	21.4	3.40	2.52	0.719	0.241	0.068	0.35	0.56
0.40	1		5.54	17.3	3.13	2.04	0.618	0.290	0.078	0.45	0.51
2	0.05		3.99	10.0	2.52	1.18	0.529	0.472	0.647	0.68	0.40
1	0.10		5.41	16.7	3.08	1.99	0.658	0.345	0.209	0.49	0.45
0.20	0.50	8.50	7.16	26.6	3.71	3.17	0.826	0.140	0.029	0.20	0.72
0.10	1		7.53	28.9	3.84	3.40	0.864	0.104	0.014	0.15	0.78
0.02	5		7.76	30.4	3.92	3.58	0.886	0.073	0.003	0.11	0.84
0.40	0.50	2.00	1.64	2.27	1.39	1.14	0.847	0.614	0.458	0.43	0.72
0.40	0.50	5	3.73	8.96	2.40	1.79	0.750	0.338	0.142	0.38	0.58
0.40	0.50	10	7.39	28	3.79	2.80	0.712	0.217	0.055	0.34	0.56
0.40	0.50	50	37.2	415	11.1	8.29	0.657	0.077	0.006	0.27	0.60

stroke. The net amount of mechanical work given to the gas in this example is $\tilde{W}(0) = 0.102$. The parameter for total energy loss takes a maximum value $\tilde{L} = 0.194$ at $\xi = 0.2$, when the heat-transfer rate becomes zero, and the free-stream temperature ratio T_∞/T_1 is nearly unity. The heat-transfer calculation is not correct beyond $\xi \simeq 0.64$ in the reverse stroke, since $\psi > 0.5$; the computed values for density and temperature are therefore not listed here.

Computed variations in the heat-transfer rate and the boundary-layer thickness with piston position are shown in Fig. 2. The thickness function ψ shows an insignificant local maximum in the forward stroke near $\xi = 0.2$ (with $T_\infty/T_1 \sim 1.10$). The computed heat-transfer rate has a very sharp maximum at $\xi = 1.0$ and shows significant asymmetry around $\xi = 1.0$.

Further numerical results are presented in Table 2. Characteristic data for the piston turning point are listed here, together with the computed piston position $\eta(\tilde{q} = 0)$ when the heat-transfer rate becomes zero in the return stroke, which with this zero-parameter model occurs when $T_\infty/T_1 = 1.0$. The final pressure $p(\xi = 0)/p_1$, which is equal to $E(\xi = 0)/E_1$, is listed as well. The data is presented in four groups, the first group showing the effect of ϵ-variation, keeping other parameters constant, including the piston-kinematics function $g(\xi)$. We find for increasing values of ϵ that the computed peak pressure and energy ratios decrease strongly. For example, in the first group for $\epsilon = 0.80$, the energy ratio is as low as $E/E_1 = 1.56$ with $T_\infty/T_1 = 2.81$ at $\eta = 1.0$, compared to $E/E_1 = 4.16$ for no losses. It should be noted that although $\psi(\xi = 1.0) < 0.5$ in this group, the small-thickness assumption was violated during part of the forward stroke for values $\epsilon \geq 0.40$. Violation occurred in the range $0.05 < \xi < 0.29$ for $\epsilon = 0.60$, and with a local peak value of $\psi(\xi = 0.18) = 0.89$. The significance of such a partial violation to the computed conditions at the end of the forward stroke is judged to be small, due to the small temperature rise in the gas ($T_\infty/T_1 = 1.071$ at $\eta = 0.18$ for $\epsilon = 0.60$).

The effect of a variation in the geometrical parameter d_0/D, keeping other parameters constant, is shown in the second group of Table 2. An increased value d_0/D will decrease p/p_1 and E/E_1 at the piston turning point. A pure variation in compressor-head geometry, i.e., changing d_0 with D and V_1/V_0 constant, is shown in the third group of Table 2. Both ϵ and d_0/D are varied in such a way that their product is constant. It is obvious that lowering d_0/D (i.e., increasing the wetted area A_0 of the compression head keeping the volume V_0 and D constant) the peak pressure ratio p/p_1 and the energy ratio E/E_1 both decrease, and the thickness parameter $\psi(\xi = 1.0)$ increases. The computations reveal that the peak in the energy ratio E/E_1 occurs before the turn of the piston, e.g., a peak $E/E_1 = 1.28$ at $\xi = 0.970$ for the calculation with $\epsilon = 2.0$ and $d_0/D = 0.05$ in the third group of Table 2. The fourth group of Table 2 shows the effect of a variation in V_1/V_0. It is interesting to see that increasing V_1/V_0, the work addition parameter $\tilde{W}(\xi = 1.0)$ is lowered due to heat losses, but the boundary-layer thickness function is smaller as well. For a high volumetric compression ratio, such as for $V_1/V_0 = 50$, the cold boundary layers can naturally hold a very large amount of dense gas.

III. Experiment

Apparatus

A small piston gas compressor was specially designed and built for study of the heat-transfer losses. The experimental apparatus is shown in the schematic drawing of Fig. 3

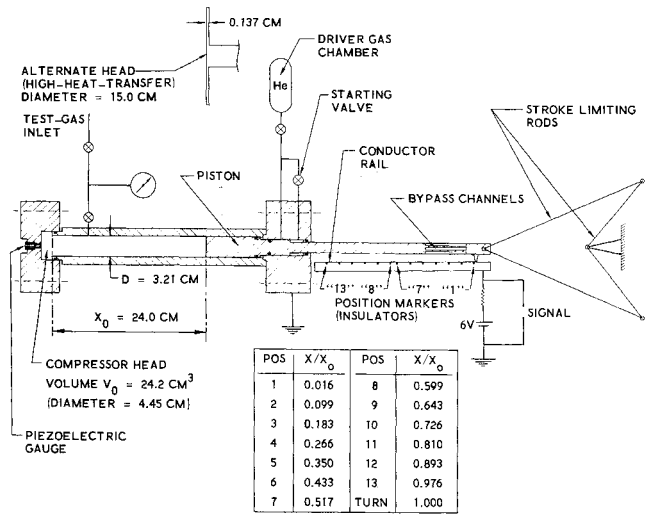

POS	X/X_0	POS	X/X_0
1	0.016	8	0.599
2	0.099	9	0.643
3	0.183	10	0.726
4	0.266	11	0.810
5	0.350	12	0.893
6	0.433	13	0.976
7	0.517	TURN	1.000

Fig. 3 Schematic drawing of experimental apparatus.

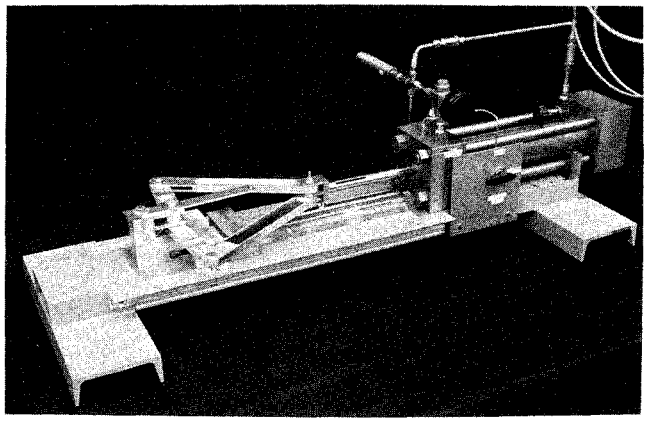

Fig. 4 Photograph showing the experimental apparatus. The stroke limiting rod arrangement is shown at the left, and the compressor used at the right.

and the photograph of Fig. 4. The compression tube was made of steel with a diameter of $D = 32.1$ mm i.d.; the piston stroke was $x_0 = 240$ mm. Two different compression heads were used, each with a volume of $V_0 = 24.2$ cm^3. The low-heat-transfer head with steel walls was cylindrically shaped with 44.5 mm i.d. and 15.6 mm depth, giving a wetted surface area of $A_0 = 52.9$ cm^2, and $d_0/D = 0.57$. The second head designed for very high heat losses was made of copper, and had 150 mm i.d. with 1.37 mm depth, giving the much larger cooling area of $A_0 = 360$ cm^2, and $d_0/D = 0.084$. With the high-heat-transfer head the computed boundary-layer thickness rapidly exceeded the 1.37 mm depth, and the present theory, therefore, was not applicable. However, the experimental results for this head are interesting and are reported here for completeness.

The theoretically designed value for the compressor volumetric compression ratio was $V_1/V_0 = 9.0$. Because of movements of compression-head O-rings during the final part of high-pressure compression, and due to finite piston clearance, the actual compression ratio was lowered to typically $V_1/V_0 = 8.6 \pm 0.1$ for the low-heat-transfer head, and to $V_1/V_0 = 8.3 \pm 0.1$ for the high-heat-transfer head.

The piston was made of leaded steel and coated on its cylindrical surface with a thin layer of spraycoated brass material, which was machined and polished to give a maximum clearance of 0.05 mm to the honed steel compression tube. The cylindrical surface of the piston had 84 mm length

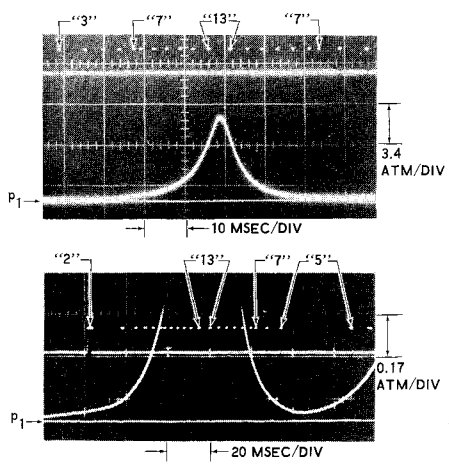

Fig. 5 Typical oscilloscope pressure records (with different sensitivities) of an experiment with the low heat-transfer head. Upper beam is the piston-position signal. Test gas helium, initial pressure $p_1 = 0.340$ atm. Measured peak pressure ratio $p_{max}/p_1 = 21.9$.

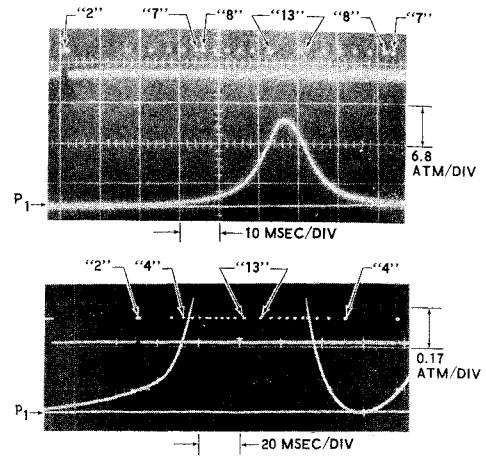

Fig. 6 Oscilloscope pressure records of an experiment with the low-heat-transfer head and helium as test gas, initial pressure $p_1 = 0.680$ atm. Measured peak pressure ratio $p_{max}/p_1 = 22.7$.

with a spring-loaded dry teflon seal facing the driver gas, as indicated in Fig. 3. This piston assembly was used successfully for well over 150 tests, with no visible sign of damage. The piston seal was periodically checked and found adequate for handling pressures down to $p_1 = 10$ μHg of test gas, and up to the maximum employed 50 atm pressure for the helium driver gas.

The piston was driven forward by high-pressure helium driver-gas, which was manually released into the driver volume from a storage chamber by the valve mechanism shown in Fig. 2. The stroke-limiting rod assembly of aluminum forced the piston to turn at the predetermined point, and subsequently to perform a reverse stroke. After completion of the major part of the forward stroke, driver gas was exhausted through the bypass channels near the end of the piston rod, when these channels exposed the driver volume to the ambient air. A relatively rapid throw-back of the piston was then assured. Frequently, one or two additional oscillations occurred before the piston assembly stopped and the energy was completely dissipated. The motion of the piston rods was generally too rapid to be visually observed; the stroke-limiting rods were therefore marked and their initial and final positions registered in each experiment in

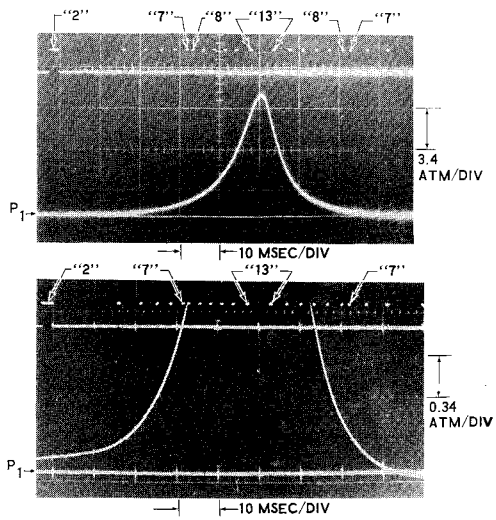

Fig. 7 Oscilloscope pressure records of an experiment with the high-heat-transfer head. Test gas helium, initial pressure $p_1 = 1.02$ atm. Measured peak pressure ratio $p_{max}/p_1 = 11.2$.

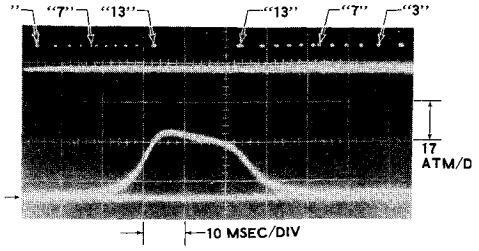

Fig. 8 Oscilloscope pressure record of an experiment with the low-heat-transfer head. Test gas argon, initial pressure $p_1 = 1.02$ atm. The effect of heat transfer is visible, e.g., from the difference in pressures in "forward" and "reverse" strokes at position "13."

order to check that proper "cross-over" of the linkage arms had occurred.

The test gas was injected into the compressor volume after repeated flushing with test gas and intermediate evacuation of the compressor volume. The initial pressure was measured with a precision Bourdon gauge with better than 0.5% accuracy. The initial gas and compressor-wall temperatures were 22 ± 2°C.

The time history of the test-gas pressure in the compression head was recorded on an oscilloscope during the piston motion, using a flush-mounted piezoelectric pressure transducer (acceleration-compensated Kistler Model 602R with silicon rubber coating for thermal protection). The piston position in the tube was recorded simultaneously by displaying discrete voltage signals, obtained with an electric contact arrangement, as shown in Fig. 3. The electrically grounded contact was attached to the piston assembly, and performed a linear sliding motion over a d.c.-charged metallic rail, containing narrow, 1.5-mm-wide, insulator slits. When the contact passed over the insulator region, a 6 v d.c. signal was displayed on the oscilloscope. Thirteen insulator slits were used. The slit spacing was 20 mm, except 10 mm between the "7" and "8" slits (see table in Fig. 3). The irregularity in spacing permitted positive identification of the origin of the recorded signals.

Experimental Results

Experiments were conducted with helium and argon test gases, and with initial pressures in the range 20 mm Hg $\lesssim p_1 \lesssim$ 2 atm. The forward stroke times were typically $20 < \tau < 100$ msec. The measured peak velocities of the piston were smaller than 15 m/sec, and much smaller than the speed of sound in the test gas. As expected, presence of shock waves within the gas were not recorded by the pressure gage; the recorded profiles were smooth. The piston kinematics generally showed piston acceleration to position "6" at $\xi = 0.43$, thereafter a relatively constant piston velocity to position "11" at $\xi = 0.81$, after which followed a rapid piston deceleration and reverse motion. The first part of the reverse motion was nearly symmetric with the forward stroke in time. The later motion was slower, and with new forward stroke starting typically near the "2" or "3" positions ($\xi = 0.10$ and $\xi = 0.18$, respectively).

Examples of oscilloscope records are shown in Figs. 5-8. We see that the presence of heat-transfer losses is manifested by a substantial lowering of the peak gas pressure from the isentropic value, and lower gas pressures of the reverse motion than in the forward motion. The observed lowering of the pressure and hence also the average energy density of the gas in the reverse stroke was in some cases so significant that the recorded pressure fell substantially below the initial value p_1 at positions "2" or "3." This effect was most evident with the high-heat-transfer head. In principle, such cooling could be used for refrigeration purposes.

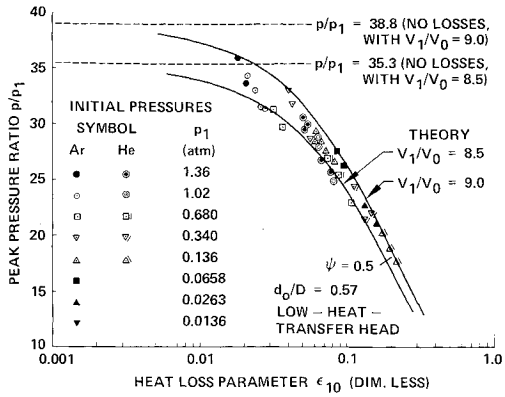

Fig. 9 Collected data for the measured peak pressure ratio with both helium and argon test gases and the low-heat-transfer head. The data are plotted vs the dimensionless heat-loss parameter ϵ_{10}, defined as $\epsilon_{10} = \epsilon(1 - \tilde{t}_{10})^{1/2}$. Excellent agreement is found with the theoretical predictions.

A wide range of compressions were studied with the experimental apparatus, covering loss-dominated compressions (e.g., with helium and the high-heat-transfer head) as well as compressions with small-to-moderate effect of heat transfer (e.g., with argon and low-heat-transfer head). With the low-heat-transfer head the measured peak pressure ratios were in the range $15 \lesssim p/p_1 \lesssim 30$, and with the high-heat-transfer head in the range $10 \lesssim p/p_1 \lesssim 20$; the isentropic peak pressure ratio is $p/p_1 = 35.3$ for $\gamma = \frac{5}{3}$ and $V_1/V_0 = 8.5$. Helium gave lower peak pressure ratios than argon, since the thermal conductivity for helium is approximately 8.6 times larger than for argon and the anticipated energy loss rate correspondingly higher for helium. A few tests with helium of initial pressure $p_1 = 20$ mm Hg and the high-heat-transfer head gave as low peak pressure ratios as $p/p_1 \simeq 9.8$, indicating that the mean gas temperature near the piston bounce was only slightly higher than the initial temperature T_1.

Estimates indicate that the wall-temperature rise in the experiments were of the order of 1°K due to the heat transfer from the gas. For practical purposes the wall temperature could therefore be considered constant, as assumed in the analysis.

Experimental peak-pressure data for helium and argon with the low-heat-transfer head are presented jointly in Fig. 9, and for the high-heat-transfer head in Fig. 10. The

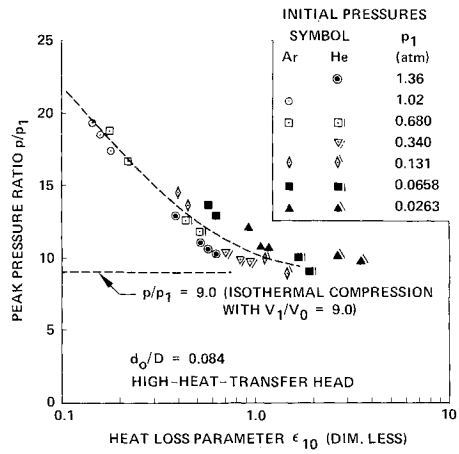

Fig. 10 Collected data for the measured peak pressure ratio with helium and argon test gases with the high-heat-transfer head. Here, the present theory cannot be used for correlation.

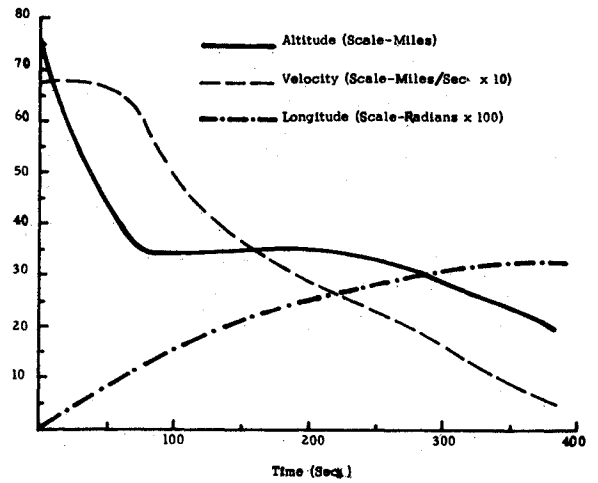

Fig. 1 State variables r, θ, and V for optimal, constrained re-entry.

$$\Delta h_2 = (\partial h_2/\partial \lambda_u)\,\Delta\lambda_u + (\partial h_2/\partial v_2)\Phi(2,1)(\partial v_1/\partial z_1)\Phi_2(1,0) \times \delta\lambda_0 + (\partial h_2/\partial v_2)\Phi(2,1)[(\partial v_1/\partial z_1)\dot{z}_1 - \dot{v}_1]\,\Delta t_1 + (\partial h_2/\partial v_2)\dot{v}_2\Delta t_2 \quad (46)$$

$$\Delta h_f = \bar{\Phi}(f,2)\,\Delta\lambda_u + \bar{\Phi}(f,2)\Phi(2,1)(\partial v_1/\partial z_1)\Phi_2(1,0)\,\delta\lambda_0 + \bar{\Phi}(f,2)\Phi(2,1)[\partial v_1/\partial z_1\dot{z}_1 - \dot{v}_1]\,\Delta t_1 + [\bar{\Phi}(f,2)\dot{v}_2 - \partial h_f/\partial z_f\Phi(2,1)\dot{z}_2]\,\Delta t_2 + \dot{h}_f\Delta t_f \quad (47)$$

where

$$\bar{\Phi}(f,2) = \partial h_f/\partial z_f\Phi(f,2)B_1 \quad (48)$$

and

$$B_1{}^T = \left[\begin{array}{cccccc|cccccc} 0 & 1 & 0 & 0 & 0 & 0 & & & & & & \\ 0 & 0 & 1 & 0 & 0 & 0 & & & & & & \\ 0 & 0 & 0 & 1 & 0 & 0 & & & 0 & & & \\ 0 & 0 & 0 & 0 & 0 & 1 & & & & & & \\ \hline & & & & & & 0 & 1 & 0 & 0 & 0 & 0 \\ & & & & & & 0 & 0 & 1 & 0 & 0 & 0 \\ & & & 0 & & & 0 & 0 & 0 & 1 & 0 & 0 \\ & & & & & & 0 & 0 & 0 & 0 & 0 & 1 \end{array}\right]$$

B_1 is a 12×8 matrix, and $\bar{\Phi}(f,2)$ is a 6×8 matrix. Also,

$$\bar{\Phi}(f,2) = (\partial h_f/\partial z_f)\Phi(f,2)B_2 \quad (49)$$

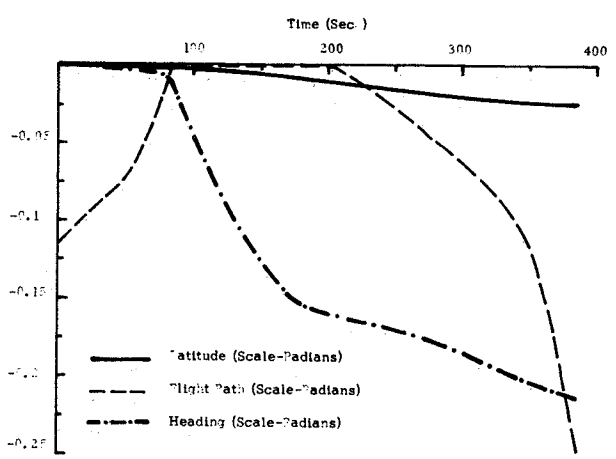

Fig. 2 State variables ϕ, γ, and ψ for optimal, constrained-re-entry trajectory.

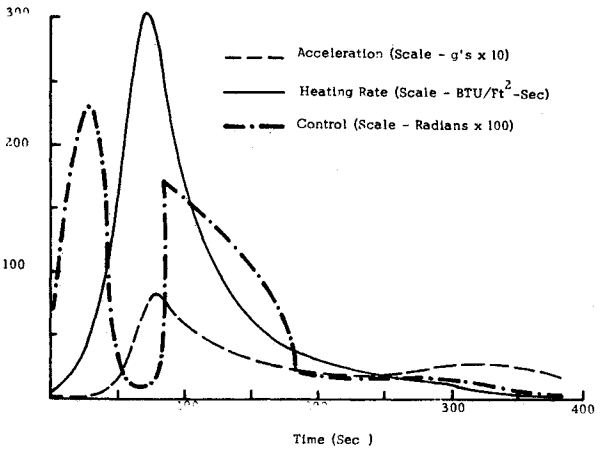

Fig. 3 Control, acceleration, and heating rate for optimal re-entry trajectory.

where

$$B_2{}^T = \begin{bmatrix} 0 & 0 & 0 & 0 & 0 & 0 & 1 & 0 & 0 & 0 & 0 & 0 \\ 0 & 0 & 0 & 0 & 0 & 0 & 0 & 0 & 0 & 0 & 1 & 0 \end{bmatrix}$$

B_2 is a 12×2 matrix, and $\bar{\Phi}(f,2)$ is a 6×2 matrix.

Thus, $\Phi(f,2)$ separates out the coefficients for $\Delta\lambda_u$, and $\bar{\Phi}(f,2)$ includes the other terms after realizing that Δr_2 and $\Delta\gamma_2$ are zero. All other terms correspond directly to the previous development.

The numerical values for the initial conditions are $r_0 = 4035.758$ miles (400,000 ft), $\theta_0 = 0.0$ rad, $\phi_0 = 0.0$ rad, $V_0 = 6.8181818$ miles/sec (36,000 fps), $\gamma_0 = 0.1134464$ rad ($-6.5°$), and $\psi_0 = 0.0$ rad. The terminal conditions are $\theta_{fs} = 0.33$ rad, $\phi_{fs} = -0.025$ rad, and $V_{fs} = 0.5$ miles/sec.

The initial multipliers for the unconstrained trajectory shown in Ref. 12 will be used as initial multipliers for the iteration procedure here. These values, guesses for the unknown vector λ_u, and guesses for t_1, t_2, and t_f are shown in Table 1. The constraint altitude chosen is $r_d = 3995.0$ miles. The same numerical integrator discussed earlier is used here.

Approximately 32 sec of computer time on the CDC 6600 is required for each iteration of the constrained re-entry trajectory. The method requires 104 iterations to converge. Plots of the states, control, acceleration, and heating rate are shown in Figs. 1–3.

The modified MPF does very well for the first few iterations, and then the norm begins to decrease very slowly for a considerable number of iterations. Over this interval, the signs on the corrections of most of the variables oscillate back and forth from plus to minus. Elements of the linear system produced by the transition matrices change only in about the third or fourth digits. The flight-path angle at t_f over this interval is near $-60°$. It is changing very rapidly near the end of the trajectory, and, if the equations are integrated for a few more seconds past the nominal final time, it quickly approaches $-90°$. A singularity exists in the equations at $-90°$, and accurate integration near this singularity is very difficult. The iteration continues for about 70 iterations, slowly increasing γ. After the flight-path angle is changed to $-35°$, the method begins to converge very rapidly again.

Another problem is that large corrections oscillating from plus to minus are calculated at t_2. The control along the boundary segment is calculated from Eq. (36). If the time calculated for t_2 is sufficiently large, the velocity along the boundary becomes small enough to make the absolute value of $\cos\beta$ greater than one. This indicates that the vehicle cannot fly at a specified altitude for an infinite time interval. If the value of t_2 is larger than the maximum time interval

part of the forward stroke, e.g. given by $\psi(\xi = 0.5) = 0.241$, and again thicker in the reverse stroke than for piston turning, with breakdown at $\xi = 0.79$ (in a fashion much similar to that shown in Fig. 2).

A large number of detailed comparisons of experimental and theoretical pressure profiles were made with helium and argon test gases, using the measured correct piston kinematic function $g(\xi)$ as input to the numerical analysis. In all cases, the computed theoretical profiles correlated surprisingly well with experiments, and confidence established in the present theoretical model.

IV. Concluding Remarks

The analysis of gas heating characteristics in a piston compressor with energy losses, which was based upon a chosen value

$$f'(\eta = 0)\int_0^\infty f(\eta)d\eta = -1.0$$

for a zero-order similarity boundary-layer profile, was found to predict the pressure-time history of such compressions to remarkably good agreement with the experiments. In the present set of experiments, the heating was relatively small with peak temperatures of $T \lesssim 1300°K$ in helium and argon. The theory may in certain cases be extended to yield results for much higher compression ratios and temperatures, e.g. to $T = 5000°K$ and higher, as experienced in advanced piston compressors for shock tubes and shock tunnels. Naturally, proper account should then also be taken of possible real-gas effects and energy losses through the mode of radiation. For the shock-tube applications, the present zero-parameter similarity approach could be sufficiently accurate to predict energy loss characteristics of slow forward piston motion in the compressor; characteristics of a possible reverse piston motion are generally of little or no interest to these applications. When the present computational scheme is applied, one should carefully check the assumptions that the piston velocity is indeed much smaller than the speed of sound of the gas, that the thermal boundary layer is of a laminar nature, and also that the small-thickness assumption for the boundary layer is not violated in any phase of the forward stroke, although at the piston turning point the boundary layer may be temporarily thick, as demonstrated in this paper. For the bypass piston tube (a high-performance piston gas heater studied by Knöös[2]), in which gases can be heated to temperatures above 10,000°K, an initial high-speed injection of gas into the compression tube and vortex formation with turbulence may prevent the unconditional application of the present scheme for calculation of energy losses. However, in the final part of the compression of gas in the bypass piston tube, the turbulence may not be present and the analysis applicable, preferably in a modified mode to include radiative losses.

For application to devices such as general piston compressor machinery, gas expansion refrigerators using reciprocating pistons, and possibly also closed-cycle hot-gas engines, e.g., of the Stirling type, the present type of analysis could give adequate prediction of the irreversible effects of heat transfer. However, great care should be exercised in the computations when the value for the freestream temperature T_∞ is nearly equal to the wall-temperature value, e.g. in an expansion process, since the boundary layer thickness parameter δ then will become infinitely large, provided that the dimensionless function G is not zero [Eq. (13)]. In computing the over-all effect of heat transfer, the thickness parameter ψ can be permitted to take values temporarily much larger than unity, provided that the free stream and wall temperatures are nearly equal. In situations with both positive and negative values of the time-derivative of the gas pressure, a logical extension and refinement of the present theory would involve a one-parameter similarity profile, in direct analogy to the method of von Kármán and Pohlhausen for two-dimensional steady-flow viscous boundary layers. Analysis with such a profile would mean a considerable complication and require larger computational efforts, but could logically be the subject for future study.

References

[1] Williard, J. W., "Design and Performance of the JPL Free-Piston Shock Tube," Fifth Hypervelocity Techniques Symposium, Univ. of Denver, March 1967, Denver.

[2] Knöös, S., "Bypass Piston Tube, a New Device for Generating High Temperatures and Pressures in Gases," *AIAA Journal*, Vol. 6, No. 4, April 1968, pp. 632–641.

[3] Knöös, S., "Study of a Bypass Piston Shock Tube," *Proceedings of the Seventh International Shock Tube Symposium*, June 1969, Toronto, Canada.

[4] Lord Rayleigh, *Philosophical Magazine*, Vol. 21, 1911, p. 697.

[5] Van Dyke, M. D., "Impulsive Motion of a Infinite Plate in a Viscous Compressible Fluid," *Zeitschrift für Angewandte Mathematik und Physik*, Vol. 3, 1952, p. 343.

[6] Knöös, S., "Boundary-Layer Structure in a Shock-Generated Plasma Flow," *Journal of Plasma Physics*, Vol. 2, Pt. 2, 1968, pp. 207–255.

[7] Schlichting, H., *Boundary Layer Theory*, Pergamon Press, New York, 1955.

[8] Westenberg, A. A., "A Critical Survey of the Major Methods for Measuring and Calculating Dilute Gas Transport Properties," *Advances in Heat Transfer*, Vol. 3, Academic Press, New York, 1966.